Crystallization of tetrahedral patchy particles in silico

Flavio Romano, Eduardo Sanz, and Francesco Sciortino

Articles you may be interested in

Understanding tetrahedral liquids through patchy colloids
J. Chem. Phys. **139**, 234901 (2013); 10.1063/1.4840695

"Ideal glassformers" vs "ideal glasses": Studies of crystal-free routes to the glassy state by "potential tuning" molecular dynamics, and laboratory calorimetry
J. Chem. Phys. **138**, 12A549 (2013); 10.1063/1.4794787

Unidirectional crystallization of charged colloids
AIP Conf. Proc. **1512**, 22 (2013); 10.1063/1.4790895

Nucleation barriers in tetrahedral liquids spanning glassy and crystallizing regimes
J. Chem. Phys. **135**, 124506 (2011); 10.1063/1.3638046

The stability of a crystal with diamond structure for patchy particles with tetrahedral symmetry
J. Chem. Phys. **132**, 234511 (2010); 10.1063/1.3454907

NEW Special Topic Sections

NOW ONLINE
Lithium Niobate Properties and Applications:
Reviews of Emerging Trends

Crystallization of tetrahedral patchy particles *in silico*

Flavio Romano,[1,a)] Eduardo Sanz,[2] and Francesco Sciortino[3]
[1]*Dipartimento di Fisica, Università di Roma La Sapienza, Piazzale A. Moro 5, 00185 Roma, Italy*
[2]*SUPA, School of Physics and Astronomy, University of Edinburgh, Mayfield Road, Edinburgh EH9 3JZ, United Kingdom*
[3]*Dipartimento di Fisica and CNR–ISC, Università di Roma La Sapienza, Piazzale A. Moro 5, 00185 Roma, Italy*

We investigate the competition between glass formation and crystallization of open tetrahedral structures for particles with tetrahedral patchy interactions. We analyze the outcome of such competition as a function of the potential parameters. Specifically, we focus on the separate roles played by the interaction range and the angular width of the patches, and show that open crystal structures (cubic and hexagonal diamond and their stacking hybrids) spontaneously form when the angular width is smaller than about 30°. Evaluating the temperature and density dependence of the chemical potential of the fluid and of the crystal phases, we find that adjusting the patch width affects the fluid and crystal in different ways. As a result of the different scaling, the driving force for spontaneous self-assembly rapidly grows as the fluid is undercooled for small-width patches, while it only grows slowly for large-width patches, in which case crystallization is pre-empted by dynamic arrest into a network glass. © *2011 American Institute of Physics*. [doi:10.1063/1.3578182]

I. INTRODUCTION

Crystallization and glass formation compete when a liquid is cooled deeply below the melting temperature. To gain control over this competition, it is essential to understand which factors favor either outcome. For instance, compositional diversity favors glass formation over crystallization in metallic alloys[1] as well as in hard-sphere colloids.[2,3] For systems composed of particles whose interaction comprises an orientationally dependent attraction, it remains as yet unclear why glass formation prevails in some instances and crystallization in others.

Here, we investigate by means of computer simulations the competition between crystallization and glass formation for spherical particles whose surface is decorated with attractive patches distributed in a tetrahedral fashion. In addition to providing fundamental understanding of the crystallization versus vitrification competition for particles interacting via an anisotropic attraction, the study of this model is particularly relevant due to the presence of a diamond cubic crystal (DC), amidst other open locally tetrahedral structures, in its equilibrium phase diagram.[4,5] A DC structure built with colloids is predicted to have important photonic properties and hence a wide range of potential applications.[6] Although several ways have been proposed to realize a colloidal diamond via the self-assembly of isotropic colloidal particles, no experimental realization has been reported so far, either because the model potential is very hard to encode into particle properties[7] or because a patterned surface is needed to trigger the self-assembly process.[8] As it is now possible to engineer patchy colloids,[9–11] a computational investigation into the possibility of obtaining a DC via the self-assembly of tetrahedral

patchy particles is especially relevant. Moreover, a study of the glass–crystal competition for low-valence patchy particles can be relevant for the challenge of protein crystallization;[12–15] our study could, for example, provide hints as to why globular proteins with hydrophobic (attractive) patches crystallize in some cases and form amorphous aggregates in others.

Numerical studies of particles with intrinsic tetrahedral symmetry[4,5,16–20] have never observed spontaneous crystallization into a tetrahedral, low-density crystal, except for one specific case reported in Ref. 21, where only a single set of parameters was studied. In this article, we identify the long sought optimal conditions for crystallization of tetrahedral colloids, providing accurate information for the design of particles that will spontaneously assemble into an open tetrahedral structure. To do so, we study the equilibrium phase behavior and the kinetics of crystallization as a function of both the patch angular width and the interaction range. We find that glass formation is favored for wide patches, whereas open tetrahedral crystals are formed for narrow ones. The interaction range has little effect on the glass–crystal competition. The different ways in which the crystallization driving force varies with the interaction parameters for the different phases (fluid and solid) explains and justifies our observations.

II. MODEL AND METHODS

A. Model

We study the Kern–Frenkel (KF) model[22] with four patches. In this model, it is possible to vary the interaction range δ and the angular width 2θ of the patch independently. In the Kern–Frenkel model,[22] each colloidal particle is described as a hard sphere of diameter σ (the unit of length) with
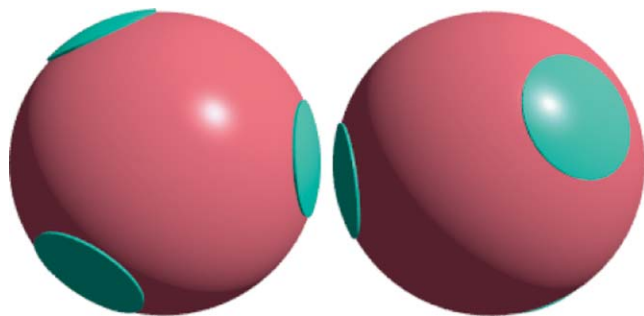
FIG. 1. Cartoon of two patchy particles modeled via the Kern–Frenkel potential. The four patches are arranged in a tetrahedral geometry. In this model, two particles are bonded with energy u_0 when the line connecting the two particle centers crosses two different patches and the center-to-center distance is less than $\sigma(1+\delta)$.

a surface decorated by four circular patches of angular width 2θ, arranged in a tetrahedral geometry. A bond of energy u_0 (the unit of energy) between two particles exists when their relative distance is smaller than $\sigma(1 + \delta)$ and any two patches on distinct particles face each other. The patches are defined by the intersection of a cone of aperture θ originating from the center of the particles with the particle surface. Specifically, the pair interaction $u(i, j)$ between particles i and j is written as the sum of a hard core potential u_{HS} and an attractive well potential of depth u_0, modulated by a function which depends only on the relative orientation of the two particles,

$$u(i, j) = u_{HS}(i, j) - u_0 f(i, j), \qquad (1)$$

where u_{HS} has the usual form

$$u_{HS} = \begin{cases} \infty, & \text{if } r_{ij} < \sigma \\ 0, & \text{otherwise} \end{cases} \qquad (2)$$

and $f(i, j)$ is a function that is always zero except when the vector joining the centers of the two particles passes through a patch on each of the particles and the distance r_{ij} is less than $\sigma(1 + \delta)$, in which case $f(i, j) = 1$. Throughout the article, pressure P is measured in units of u_0/σ^3, temperature T in units of u_0/k_B where k_B is the Boltzmann constant, and number density ρ in units of σ^{-3}. A pictorial representation of the model is given in Fig. 1. The same model, with fixed values of θ and δ (15° and 0.1σ, respectively), was studied in Ref. 21, which reported the first case of crystallization into an open, locally tetrahedral structure.

B. Methods of evaluating the phase diagram

We calculate the fluid–crystal coexistence curves following the methodologies recently reviewed in Ref. 23. In particular, we calculate the free energy of crystal phases by thermodynamic integration from the Einstein crystal,[24] and the free energy of the fluid phase by thermodynamic integration from the ideal gas. Several different crystal structures have been considered, including the cubic diamond crystal, the hexagonal diamond crystal (DH, the crystal defined by the position of the oxygen atoms in hexagonal ice), body-centered cubic (BCC), and face-centered cubic. The set of numerical techniques reviewed in Ref. 23 allows us to obtain precise

estimates of the chemical potential of the crystal, μ_{xt}, and of the fluid phase, μ_{fluid}. We use Gibbs–Duhem integration[25] to compute the coexistence line in the P-T plane and Hamiltonian Gibbs–Duhem integration[26] to calculate the phase diagram of a new set of parameters starting from known results of a previously studied set of parameters. We perform consistency checks based on direct coexistence[27] to validate our results. Finally, we calculate the gas–liquid coexistence implementing the Gibbs ensemble technique[28] and evaluate the critical point using standard methods based on grand canonical simulations.[29]

The limit of mechanical stability of the gas phase (i.e., the spinodal line) has been estimated by means of NPT simulations evaluating the $P(V)$ curve along isotherms. The spinodal P has been operationally defined as the highest P at which the gas did not convert into a liquid within 10^6 MC sweeps (see below).

C. Identification of the crystal structure

To identify open crystalline configurations (i.e., DC, DH, or their stacking polymorphs), we employed the technique introduced in Ref. 30. To each particle i, we assign a normalized seven-component vector of complex numbers $\mathbf{q}_3(i)$ that identifies the orientation of the particle with respect to its neighbors. The nonnormalized mth component of $\mathbf{q}_3(i)$ is defined as

$$q_{3m}(i) = \frac{1}{N_b(i)} \sum_{j=1}^{N_b(i)} Y_3^m(\hat{\mathbf{r}}_{ij}), \qquad (3)$$

here $N_b(i)$ is the number of neighbors within distance $\sigma(1 + \delta)$ (the location of the first minimum of the radial distribution function), Y_3^m are the spherical harmonics with total angular momentum 3 and m ranges from -3 to 3. The procedure to identify a solidlike particle involves imposing some conditions, dependent on the crystal structure that is hypothesized, on the complex conjugate scalar product, $\mathbf{q}_3(i) \cdot \mathbf{q}_3^*(j)$, to identify a solidlike bond between particles i and j. Particle i is then identified as solidlike if it has more than a threshold value of solidlike connections. Since open tetrahedral structures are difficult to discriminate a detailed discussion is in order. Several possible open crystals can be formed with four-coordinated tetrahedral particles, the DC and DH being perhaps the best known, since they are the lattices formed by the oxygen atoms in ices Ic and Ih, respectively. In addition to this two pure structures, it is possible to generate stacking hybrids by randomly alternating planes of the two pure forms without altering the local order, i.e., all particles have four tetrahedrally arranged neighbors. A DC-like and a DH-like environment will thus not be distinguished unless information beyond the second neighbor shells is used[7] in the order parameter definition. Several order parameters have been proposed to tackle this problem (see, for example, Ref. 31 for a discussion in the context of water crystallization). Here we implement two different procedures: the boat/chair analysis and a procedure that relies on the different values of $\mathbf{q}_3(i) \cdot \mathbf{q}_3^*(j)$.

The boat/chair analysis relies on the fact that in prefect crystals with a tetrahedral arrangement, one can define sixfold rings of bonded particles, since there are no rings of bonds with fewer than six particles. Such rings can assume a chairlike or boatlike form (planar or other distorted forms are allowed in a disordered system, but not in the perfect lattices), and they can be told apart by computing the dihedral angle between all consecutive triplets of particles in the ring. If all the dihedral angles are *staggered*, $(\pi/3 + k2\pi/3, \, k = 1, 2, \dots)$, the ring is identified as chairlike. By contrast, if two of those dihedral angles are *eclipsed* $(0 + k2\pi/3, \, k = 1, 2, \dots)$ the ring is identified as boatlike. The perfect DC structure has only chairlike rings, whereas in the perfect DH structure 75% of the rings are boatlike and 25% are chairlike. By counting the number of DH- and DC-like rings, one can thus tell apart the two macroscopic structures in a fully bonded configuration. To implement this procedure, we take a configuration of a spontaneously crystallizing system, discard all particles that do not belong to the largest cluster of bonded particles and count the number of chairlike (0 eclipsed and 6 staggered dihedral angles), boatlike (2 eclipsed and 4 staggered dihedral angles) and distorted (all other cases, a very small fraction) sixfold rings. Large crystalline clusters will have a number of rings of the order of N, the maximum being $2N$ in a perfect lattice, and depending on the fraction of boatlike rings we identify the cluster as DC-like, DH-like, or a stacking of the two structures. The boat/chair criterion is a good global criterion to identify the nature of the crystal obtained by spontaneous nucleation, but does not allow a precise definition of the nature of a single particle when some of the 12 rings to which the particle should belong are missing, a very strict requirement.

The nature of the local environment of a single particle can be assessed by means of the local bond-order parameter $\mathbf{q}_3(i) \cdot \mathbf{q}_3^*(j)$. Figure 2 shows the distribution of values of $\mathbf{q}_3(i) \cdot \mathbf{q}_3^*(j)$ for DH and DC crystals. In the perfect DC structure, all four neighbors (labeled by j) of particle i are such

that $\mathbf{q}_3(i) \cdot \mathbf{q}_3^*(j) = -1$, whereas in the DH structure each particle i has three neighbors such that $\mathbf{q}_3(i) \cdot \mathbf{q}_3^*(j) = -1$ and one such that $\mathbf{q}_3(i) \cdot \mathbf{q}_3^*(j) = -0.115$. We then choose to identify a bond between particles i and j as solidlike if $-1 \leq \mathbf{q}_3(i) \cdot \mathbf{q}_3^*(j) < -0.87$ or $-0.3 \leq \mathbf{q}_3(i) \cdot \mathbf{q}_3^*(j) < 0.1$. We define solidlike (either DC- or DH-like) particles as particles with four solidlike connections. Particles with all four connections such that $-1 < \mathbf{q}_3(i) \cdot \mathbf{q}_3^*(j) < -0.87$ are identified as DC-like and particles with three connections such that $-1 < \mathbf{q}_3(i) \cdot \mathbf{q}_3(j) < -0.87$ and one connection such that $-0.3 < \mathbf{q}_3(i) \cdot \mathbf{q}_3^*(j) < 0.1$ are identified as DH-like. We stress that the scalar product between the $\mathbf{q}_3$ of different particles[30] mixes information arising from the first nearest neighbor shell of both particles i and j and hence correlates properties of particles that are more than two bonds apart (i.e., third neighbors). It is important to note that using a threshold value of three solid bonds with $-1 \leq \mathbf{q}_3(i) \cdot \mathbf{q}_3^*(j) < -0.87$ can lead to misleading results for systems that can crystallize in both structures, since DC-like particles are more easily detected than DH-like ones. Hence one would both misidentify some DH-like particles as liquidlike and underestimate the total number of solidlike particles.

We have tested the crystal structures obtained by spontaneous crystallization with both methods, i.e., identifying the hexagonal rings and counting of the boat/chair ratio or counting the ratio of DC-like particles to DH-like particles based on the distribution of $\mathbf{q}_3(i) \cdot \mathbf{q}_3^*(j)$ values. The two methods provide comparable results. While for small system sizes ($N \leq 1000$) we observed pure DC and DH structures in a few cases, simulations with 10 000 particles always resulted in stacking hybrids, with a fraction of DC particles of 0.55 ± 0.15 over 20 simulations.

D. Monte Carlo simulations

Standard *NVT* and *NPT* Monte Carlo (MC) simulations have been performed for evaluating thermodynamic quantities. System of $N = 250$ particles for the fluid, $N = 216$ for the DC, $N = 256$ for the DH and $N = 250$ for the BCC phase have been simulated to evaluate phase coexistence lines. Larger systems of $N = 1000$ and $N = 10\,000$ particles have been simulated to investigate spontaneous crystallization for $T < T_x$, starting from equilibrium configurations close to the coexistence temperature T_x. We use as unit of time a MC sweep, defined as N attempts to translate and rotate a randomly selected particle in the *NVT* ensemble. In the *NPT* simulations, a MC sweep also includes, on average, one attempt to change V. Computational times vary depending on the diffusivity of the system, from a minimum of 10^5 to a maximum of 10^8 MC sweeps.

E. Iso-diffusivity lines

Systems of size $N = 1000$ have been studied to calculate the diffusion coefficient from the long time behavior of the mean square displacement. As commonly done, we have defined time as the number of MC sweeps.[32] In the case of patchy particles, at low T, MC and molecu-
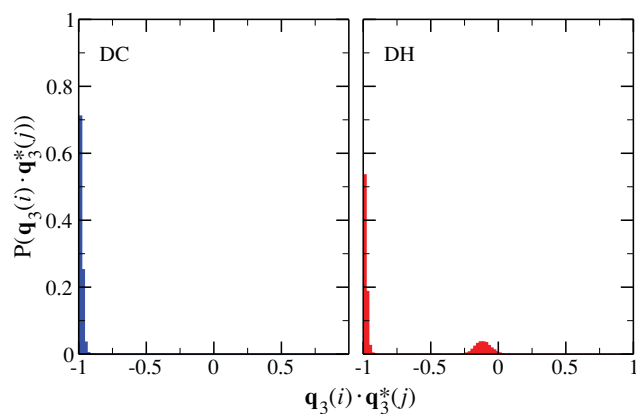
FIG. 2. Probability distribution of the complex conjugate scalar product between the local bond order parameters of two neighboring particles i and j in the DC (left) and DH (right) structures, for $\delta = 0.24$ and $\cos\theta = 0.98$. The DC distribution is peaked around -1. Only the DH distribution shows a peak around -0.1. The area under this peak is 25% of the total, indicating that DH solid particles have one out of four bonds with $\mathbf{q}_3(i) \cdot \mathbf{q}_3^*(j) \approx -0.1$ and the remaining three with $\mathbf{q}_3(i) \cdot \mathbf{q}_3^*(j) \approx -1$.
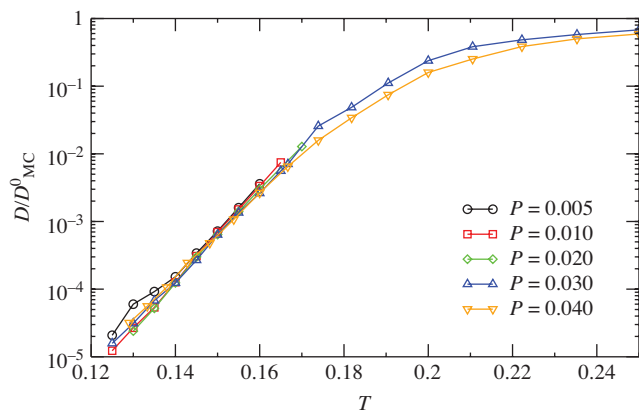
FIG. 3. Temperature dependence of the reduced diffusion coefficient along several isobars at $\theta = 23.1°$ and $\delta = 0.24$. All curves superimpose for $T < 0.18$, suggesting that the iso-diffusivity is approximately independent of the pressure and mostly controlled by T, as in previously investigated tetrahedral models (Ref. 19 and 33–36).

lar dynamics values of D show the same T-dependence.[19] In the absence of interactions, a particle evolving according to the MC scheme diffuses with a bare diffusion coefficient D_{MC}^0 controlled by the variance of the chosen random displacement along each direction.[32] Figure 3 shows the T-dependence of D/D_{MC}^0 along different isobars for $\delta = 0.24$ and $\cos \theta = 0.92$. The smallest values of D which we have been able to calculate corresponds to $D \approx 10^{-5} D_{MC}^0$. For lower T, it is impossible to equilibrate the system with present time numerical resources. The locus $D(P, T) = 10^{-5} D_{MC}^0$ provides a reasonable estimate of the dynamic arrest line for this model.

F. Functional dependence of the open-crystal entropy on θ and δ

A byproduct of the thermodynamic integration discussed in Sec. II B is the evaluation of the entropy (per particle) s_{xt} of the open crystal for a wide range of δ and θ. Due to the simple nature of the KF model, a very good approximation of the crystal entropy in its whole stability range is given by the value of the entropy at zero temperature and pressure. Its value is finite, since in this square-well-like model there are many microscopic states compatible with the fully bonded ground state. Furthermore, the entropy does not change with increasing T, since bonds do not break and the bond pattern remains identical up to the melting temperature. Since the stability field of the open crystals is limited to small P (as shown in the following), the latter is also not expected to have large effects on the entropy. We have recently studied the effect of δ on the thermodynamic behavior of tetrahedral patchy particles and found that $s_{xt} \propto 2 \ln(\delta)$.[5] We find here that the entire dependence on θ and δ can be well represented by the function (see Fig. 4)

$$s_{xt} = 2k_B \ln[(1 - \cos \theta)\delta] ,\qquad (4)$$

where $1 - \cos \theta$ is proportional to the surface fraction covered by patches. Hence, a good quality approximation for the DC/DH chemical potential at all δ and θ is provided by

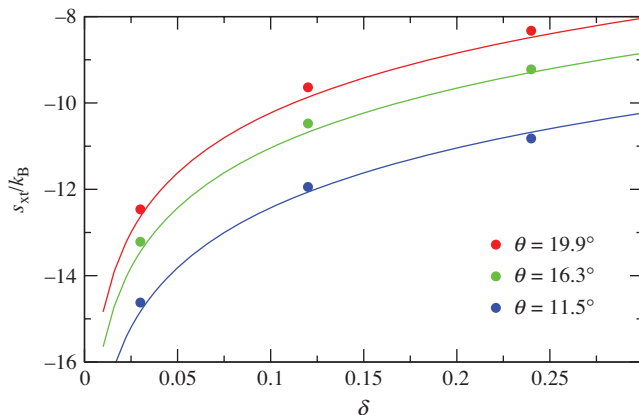$$\beta \mu_{xt} \approx -2\beta u_0 - 2k_B \ln[(1 - \cos \theta)\delta] .\qquad (5)$$

FIG. 4. Entropy of the open tetrahedral crystal at zero temperature and pressure (s_{xt}) as a function of the range δ for several values of the patch angle θ. Solid lines represent Eq. (4).

We stress that this approximation holds since the open crystal is fully bonded and hence the energy does not depend on T and the contribution of $\beta P/\rho$ is negligible throughout all its stability range.

III. RESULTS

The δ and θ pairs for which we have observed in at least one state point, i.e., for a specific choice of T and ρ, the formation of an open crystal in MC simulations are reported in Fig. 5. This figure clearly shows that open crystal structures spontaneously form only when the patch width is smaller than about 30°, almost independently of the range of the attraction. This finding is consistent with that of Ref. 21 (blue diamond in Fig. 5), which also showed the formation of open structures at a patch width of 30°.

To investigate the reasons for such sensitivity of spontaneous crystallization, we evaluate the stability field of the fluid, of the open crystals and of the BCC crystals for several
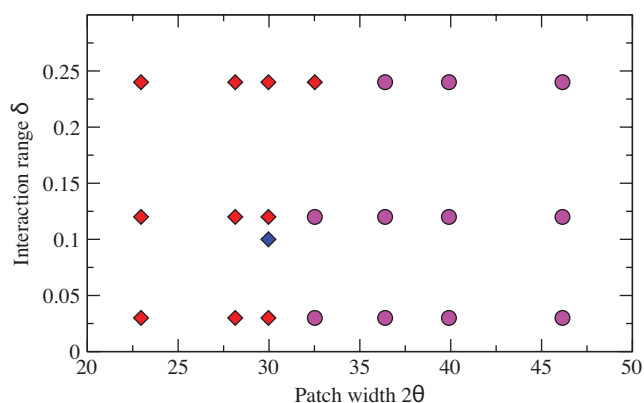

FIG. 5. Boundary between crystallizing (into an open structure) and noncrystallizing colloidal particles interacting via a four-patch tetrahedral potential. Symbols (diamonds for crystallizing and circles for glass-forming models) correspond to actual calculations for different values of the radial interaction range (δ, in units of the particle diameter) and of the angular width of the patch (2θ, in degrees), obtained by slowly cooling the fluid below the fluid-DC/DH coexistence temperature. The point studied in Ref. 21 is included (blue diamond).
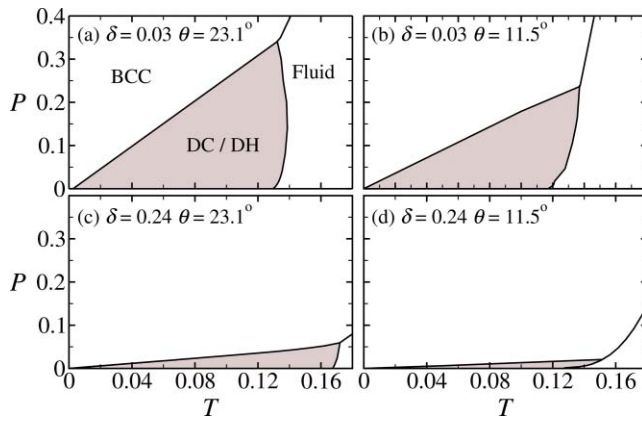
FIG. 6. Evolution of the phase diagram with the interaction range δ and the patch width 2θ. As expected—since DC and DH are roughly half as dense as BCC—they are the most stable phase at low P and T, while BCC is the most stable at low T and high P. At high T and low P, the fluid phase is stable. As δ is increased, the triple point moves toward higher T and lower P, while increasing θ moves the triple point toward higher P but the effect on T is not straightforward.

values of δ and θ using thermodynamic integration methods.[23] In our short-range attractive model, the DC and DH structures have identical density and free energy within our numerical precision of about $0.02\,k_BT$. Although this is obvious at $T = 0$, it also extends to finite T. This is not surprising, since all these open crystals are fully bonded and have the same local structure up to second neighbors. Results are reported in Fig. 6 in the pressure–temperature plane. The DC/DH stability field decreases progressively on increasing δ and decreasing θ, which would suggest that crystallization to a DC/DH structure would be disfavored for small θ, contrary to what is shown in Fig. 5.

The explanation of this puzzling result can be found by investigating the δ and θ dependence of the driving force for crystallization, i.e., the difference in chemical potential between the fluid and the crystal phases $\Delta\mu \equiv \mu_{\text{fluid}} - \mu_{\text{xt}}$, normalized by the thermal energy k_BT. Figure 7(a) shows the T-dependence of $\beta\mu_{\text{xt}}$ and $\beta\mu_{\text{fluid}}$ [where $\beta \equiv 1/(k_BT)$] along an arbitrary isobar for a crystallizing and a noncrystallizing case. The curves cross at the coexistence temperature T_x. The figure reveals that in the case of wide patches, the driving force for crystallization (the difference between the two curves) grows very moderately for $T < T_x$. By contrast, in the case of narrow patches, the slopes of $\beta\mu_{\text{xt}}$ and $\beta\mu_{\text{fluid}}$ at T_x are rather different, creating a large increase in $\beta\Delta\mu$ on supercooling.

To better grasp the different roles of θ and δ on the relative location of $\beta\mu_{\text{xt}}$ and $\beta\mu_{\text{fluid}}$, we build on the work of Wertheim,[37] which suggests that in associating liquids, the thermodynamics of the fluid state is controlled by one parameter measuring the so-called bonding volume V_b, the volume of the interaction well around each particle. For the four-patch Kern–Frenkel model, we have[38] $V_b = [(1 - \cos\theta)]^2 \times (4\pi\sigma^3/3)[(1 + \delta)^3 - 1]$. Starting from one arbitrary combination of θ and δ (model A), for which it is not possible to generate a large driving force for crystallization, we generate two other models, one by decreasing only δ (model B) and one by decreasing only θ (model C), in such a way that models B
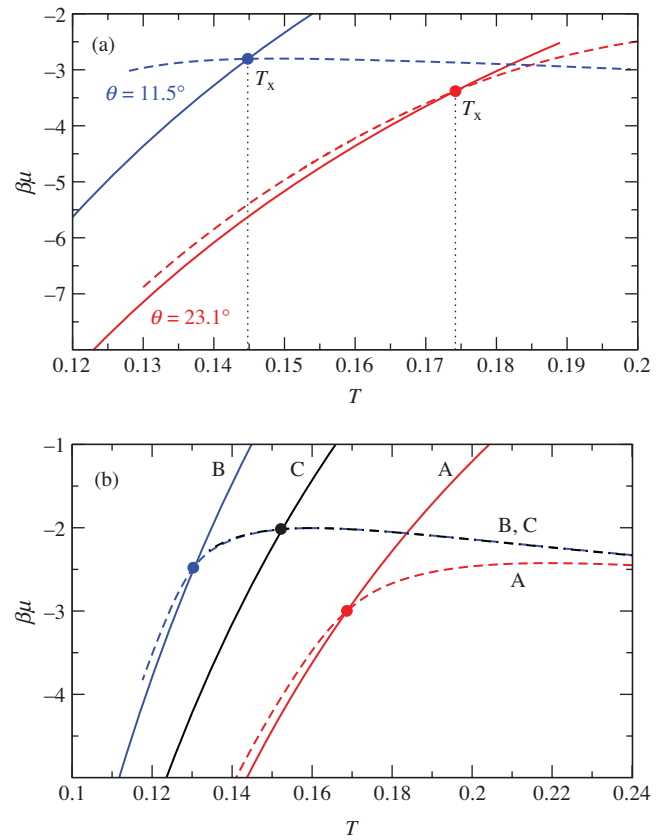

FIG. 7. Chemical potential of the fluid (dashed curves) and of the DC/DH crystal (solid curves) against T along an isobar: (a) $\theta = 11.5°$, $\delta = 0.24$ at $P = 0.01$ and $\theta = 23.1°$, $\delta = 0.24$ at $P = 0.03$. The difference between the curves below the melting temperature T_x is the driving force, which grows very sharply for $\theta = 11.5°$ and increases modestly for $\theta = 23.1°$. (b) Fluid and DC/DH chemical potentials at $P = 0.02$ for three different combinations of the potential parameters. Model A was chosen arbitrarily ($\theta = 19.9°$, $\delta = 0.24$), while model B ($\theta = 19.9°$, $\delta = 0.0325$) has the same θ as model A and model C ($\theta = 11.5°$, $\delta = 0.24$) has the same δ as model A. Models B and C have the same bonding volume (see text), so that the thermodynamics of the fluids is identical. Note that the lowest T for which $\beta\mu_{\text{fluid}}$ is reported is controlled by spontaneous crystallization for model C and by dynamic arrest for models A and B. Large θ models (A and B) do not generate a large driving force. Note that at low T the $\beta\mu_{\text{xt}}$ curves are roughly parallel, shifted by the difference in entropy [see Eq. (4)].

and C have the same value of V_b. In agreement with Wertheim theory, our numerical calculations of $\beta\mu_{\text{fluid}}$ of model B and C superimpose, as shown in Fig. 7(b), confirming that, to a good approximation, V_b is a proper scaling variable for the thermodynamic properties of the fluid phase.

In the case of the crystal, the leading contribution to the θ and δ dependence of the chemical potential arises from the entropy, s_{xt}. Indeed, the solid is fully bonded, and the $\beta P/\rho$ contribution is small, since the DC/DH-fluid coexistence takes place at low P. As discussed in Sec. II F, s_{xt} is well represented by the expression $s_{\text{xt}} = 2k_B \ln[(1 - \cos\theta)\delta]$, and hence $\beta\mu_{\text{xt}} \approx -2\beta u_0 - s_{\text{xt}}/k_B$ has a different θ and δ dependence than that of $\beta\mu_{\text{fluid}}$, leading to different T_x and, more importantly, different slopes of $\beta\mu$ at T_x for models B and C. The slope of $\beta\mu$ as a function of T at constant P is $-\beta h/T$, where $h = u + P/\rho$ is the enthalpy and u the energy per particle. Given that the P/ρ term of h is small, the slopes of $\beta\mu_{\text{xt}}$ and $\beta\mu_{\text{fluid}}$ are essentially $\beta u_{\text{xt}}/T$ and $\beta u_{\text{fluid}}/T$,

respectively. Since the crystal is essentially fully bonded, the two slopes will be similar (small driving force on undercooling) if the fluid with which the crystal coexists is highly bonded, and substantially different (large driving force on undercooling) otherwise. In the former case, $\beta\mu_{xt}$ and $\beta\mu_{fluid}$ run almost parallel, being shifted at low T essentially by the difference in entropy $s_{xt} - s_{fluid}$, so that the driving force does not significantly grow on further cooling.

An alternative interpretation of the different crystal-forming ability for small and large θ can be expressed in terms of the difference between the fluid and crystal entropies in the fully bonded configuration. Indeed, if model C could avoid crystallization, according to Wertheim theory its fluid chemical potential would be the same as the one of model B also for $T \ll T_x$, where $\beta\Delta\mu$ coincides with $(s_{xt} - s_{fluid})/k_B$. The easily crystallizing systems are thus the ones for which the fully bonded fluid has an entropy significantly different from the one of the fully bonded crystal.

To provide evidence that the observed different T dependence in $\beta\Delta\mu$ is not sensitive to the chosen isobar, we calculate the loci (in the P–T and T–ρ planes) with the same driving force, both in the case of a crystallizing and of a noncrystallizing model. The lines in the phase

diagrams where $\beta\Delta\mu \equiv \beta\mu_{fluid} - \beta\mu_{xt}$ is constant can be calculated by implementing a straightforward extension of the Gibbs–Duhem technique. Along a line where the difference in the chemical potential between two phases, I and II, is constant, one has

$$\beta\mu_I(\beta, \beta P) = \beta\mu_{II}(\beta, \beta P) + C. \qquad (6)$$

Moving along the $\beta\Delta\mu = C$ locus, from $(\beta, \beta P)$ to $(\beta + d\beta, \beta P + d(\beta P))$, one can write

$$\beta\mu_I + \frac{\partial(\beta\mu_I)}{\partial\beta}d\beta + \partial\frac{(\beta\mu_I)}{\partial(\beta P)}d(\beta P)$$

$$= \beta\mu_{II} + C + \frac{\partial(\beta\mu_{II})}{\partial\beta}d\beta + \frac{\partial(\beta\mu_{II})}{\partial(\beta P)}d(\beta P). \qquad (7)$$

Since along the line $\beta\mu_I = \beta\mu_{II} + C$ and given the thermodynamic relations $\partial(\beta\mu)/\partial\beta = u$ and $\partial(\beta\mu)/\partial(\beta P) = v$ (v is the specific volume), one obtains

$$\frac{d(\beta P)}{d\beta} = \frac{-u_I + u_{II}}{v_I - v_{II}}. \qquad (8)$$

All the terms in Eq. (8) can be calculated by running standard *NPT* simulations of the two phases. Note that Eq. (8) is the
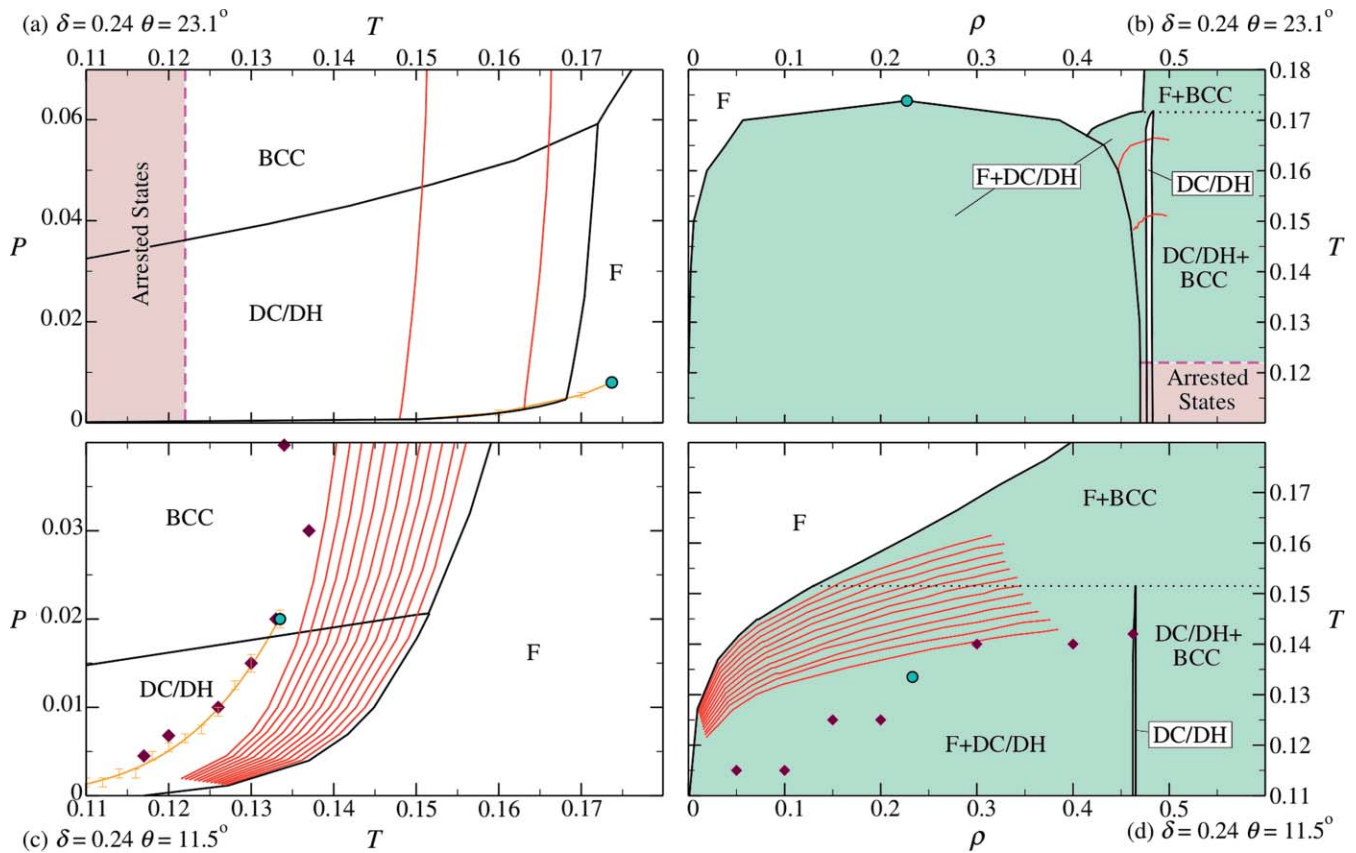

FIG. 8. P–T and T–ρ phase diagrams for crystallizing and noncrystallizing models, complemented with additional thermodynamic and kinetic information. Thick black solid lines correspond to phase boundaries. Light cyan [panels (b) and (d)] indicates phase coexistence. Phase coexistence regions are separated by dotted lines. Red solid lines represent loci with a constant driving force, $\beta(\mu_{fluid} - \mu_{xt}) = 0.1n$, with n ranging from 1 to 12. Note that $n = 0$ coincides with the fluid-DC/DH coexistence locus. At any P, the driving force grows much faster with undercooling at $\theta = 11.5°$ [panel (c)] than at $\theta = 23.1°$ [panel (a)]. Spontaneously crystallizing state points in the *NPT* or *NVT* ensembles [data available only for $\theta = 11.5°$, panels (c) and (d)] are marked with diamonds. The gas–liquid critical point is marked with a cyan circle. Spontaneous crystallization for $\theta = 11.5°$ prevents us from computing gas–liquid coexistence and hence only the limit of stability of the gas phase [orange line in panel (c)] is reported. The region of nonergodic states, bounded by the iso-diffusivity line for a reduced diffusion coefficient of $D/D_0 = 10^{-5}$ (dashed magenta), is pink shadowed in panels (a) and (b).

same that holds at coexistence ($C = 0$) and does not depend on the value of C.

Figure 8 shows that at all P, for small θ [panels (c) and (d)], iso-($\beta\Delta\mu$) curves are very densely spaced, clearly conveying the message that a small supercooling generates a significant rise in the driving force. By contrast, in the case of large θ [panels (a) and (b)], iso-($\beta\Delta\mu$) curves are widely spaced in T, confirming that it is extremely difficult to build up a reasonable $\beta\Delta\mu$ to drive crystallization. Again, this difficulty—which is present at all P—arises from the similar volume and energy of the fluid and the crystal at T_x.

Two additional pieces of information are shown in Fig. 8. First, for the large θ, noncrystallizing model, panels (a) and (b) report the iso-diffusivity line for the smallest value of the diffusion coefficient which it was possible to estimate in lengthy simulations (the computer analog of the glass line[35,38]). Indeed, the nucleation rate, besides depending on $\beta\Delta\mu$, is also affected by particle mobility and hence there is the possibility that crystallization is further suppressed for kinetic reasons. The glass transition is met when $\beta\Delta\mu$ is still small. Hence, the establishment of an extensive network of bonds is responsible not only for the similarity between the energy of the fluid and of the crystal, and thus the associated small value of the driving force, but also for the additional slowing down of the particle mobility, further decreasing the nucleation rate. Second, for the narrow patch model, panels (c) and (d) report the points where crystal formation takes place spontaneously during *NPT* and *NVT* simulations, respectively. Interestingly, for low P the crystallizing points are located just below the gas–liquid spinodal (see Sec. II), suggesting that nucleation is also possible at very small P, but requires the formation of a liquid droplet via decomposition of the gas as an intermediate step.[39,40] As soon as the liquid phase is nucleated, $\beta\Delta\mu$ is so large that spontaneous crystallization takes over.

The $T-\rho$ representation [panels (b) and (d)] is more relevant for colloidal experiments, where ρ is a better control parameter than P. For wide patches, along the gas–liquid coexistence, the driving force for nucleation is very small and thus the liquid exists as a metastable state down to the glass line. Hence, a quench into the unstable gas– liquid region will generate a gas coexisting with a weakly supersaturated liquid, or for smaller T [$T \lesssim 0.13$ for the model in Fig. 8(a)], a gas coexisting with a glass.[41] Instead, in the case of a crystallizing model (small θ), the gas–liquid coexistence is deeply metastable with respect to the fluid-DC/DH coexistence. At sufficiently large density ($\rho \gtrsim 0.3$), undercooling generates a large $\beta\Delta\mu$ that drives spontaneous nucleation. For smaller densities, crystallization is still possible, but requires gas–liquid phase separation as an intermediate step to generate large local densities.[40]

It is important to note that in the T and P range shown in Fig. 8(c), crystallization always takes place into an open crystal structure, even in state points where the most stable phase would be the BCC. This signals the presence of a much lower free energy barrier for nucleation of the open crystal with respect to that of the BCC at low P. In our opinion, this is due to the closer values of the fluid and open crystal densities, compared to the BCC which is twice as dense, resulting in a significantly lower surface tension of the DC/DH-fluid interface. As expected, at P higher than those shown, the fluid crystallizes into the BCC.

IV. DISCUSSION AND CONCLUSIONS

The different scaling of the fluid and crystal chemical potentials with θ and δ is fundamental in the interpretation of the different crystal-forming abilities of tetrahedral patchy particles. As a result of the different scaling, the driving force for crystallization rapidly grows as the fluid is cooled below T_x for small-width patches, while it only grows slowly for large-width patches, where crystallization is pre-empted by the formation of a glass state. These considerations suggest that an open tetrahedral crystal structure will be easily crafted if the colloids are engineered with patches of angular width 2θ smaller than $\sim 30°$, a requirement which appears feasible in view of the recent advances in colloidal synthesis.[9–11] Spontaneous crystallization will take place directly in a broad range of densities around the DC/DH equilibrium density and is aided by the metastable gas–liquid separation at lower densities.

As we have alluded to in Sec. I, fabrication of colloidal crystals with a diamond structure is crucial for innovative photonic applications, including inhibition of spontaneous emission, enhancement of semiconductor lasers, and integration and miniaturization of optical components.[6] Indeed, the band structure in colloidal diamonds has a wide and robust prohibited gap in the visible region, preventing propagation of light in all directions within a frequency range.[42] Techniques have been designed to build the DC structure starting with spherically interacting colloids, based on nanorobotic-driven assembly[43] or cleavage of colloidal laves.[8] Our work explores a very promising alternative for building bulk quantities of colloidal diamond: the self-assembly of *ad hoc* engineered patchy particles. Our study suggests that reaching the goal of self-assembling a colloidal diamond will require more than engineering and producing in bulk quantities tetrahedrally coordinated particles. Indeed, it will be important to add to the directional short-ranged patch–patch interaction an additional contribution to stabilize the DC structure with respect to the DH and the stacking hybrids. Again, future numerical investigation can help in answering this important question, and thus pave the way for experimental realization of a colloidal diamond via the self-assembly of patchy particles.

Finally, our study also offers a key to interpreting the different glass-forming abilities of tetrahedral network forming liquids, such as silica, silicon, and water.[44–46] Recent numerical studies[33] suggest that silica, the archetypal glass-former liquid, is characterized by a Si–Si–Si angular distribution which is wider than the corresponding O–O–O distribution of supercooled water, thus establishing a correlation between the angular width of the bond and the system's glass-forming ability.

ACKNOWLEDGMENTS

[1] K. Kelton, *Crystal Nucleation in Liquids and Glasses* (Academic, Boston, 1991).

[2] H. J. Schöpe, G. Bryant, and W. van Megen, J. Chem. Phys. **127**, 084505 (2007).

[3] E. Zaccarelli, C. Valeriani, E. Sanz, W. C. K. Poon, M. E. Cates, and P. N. Pusey, Phys. Rev. Lett. **103**, 135704 (2009).

[4] F. Romano, E. Sanz, and F. Sciortino, J. Phys. Chem. B **113**, 15133 (2009).

[5] F. Romano, E. Sanz, and F. Sciortino, J. Chem. Phys. **132**, 184501 (2010).

[6] M. Maldovan and E. L. Thomas, Nature Mater. **3**, 593 (2004).

[7] M. C. Rechtsman, F. H. Stillinger, and S. Torquato, Phys. Rev. E **75**, 031403 (2007).

[8] A. Hynninen, J. H. J. Thijssen, E. C. M. Vermolen, M. Dijkstra, and A. van Blaaderen, Nature Mater. **6**, 202 (2007).

[9] D. J. Kraft, J. Groenewold, and W. K. Kegel, Soft Matter **5**, 3823 (2009).

[10] Q. Chen, S. C. Bae, and S. Granick, Nature (London) **469**, 381 (2010).

[11] F. Romano and F. Sciortino, Nature Mater. **10**, 171 (2011).

[12] P. G. Vekilov, Soft Matter **6**, 5254 (2010).

[13] H. Liu, S. K. Kumar, and F. Sciortino, J. Chem. Phys. **127**, 084902 (2007).

[14] A. Lomakin, N. Asherie, and G. B. Benedek, Proc. Natl. Acad. Sci. U.S.A. **96**, 9465 (1999).

[15] C. Gogelein, G. Nagele, R. Tuinier, T. Gibaud, A. Stradner, and P. Schurtenberger, J. Chem. Phys. **129**, 085102 (2008).

[16] J. P. K. Doye, A. A. Louis, I. Lin, L. R. Allen, E. G. Noya, A. W. Wilber, H. C. Kok, and R. Lyus, Phys. Chem. Chem. Phys. **9**, 2197 (2007).

[17] J. Kolafa and I. Nezbeda, Mol. Phys. **61**, 161 (1987).

[18] C. Vega and P. A. Monson, J. Chem. Phys. **109**, 9938 (1998).

[19] C. De Michele, S. Gabrielli, P. Tartaglia, and F. Sciortino, J. Phys. Chem. B **110**, 8064 (2006).

[20] E. G. Noya, C. Vega, J. P. K. Doye, and A. A. Louis, J. Chem. Phys. **132**, 234511 (2010).

[21] Z. Zhang, A. S. Keys, T. Chen, and S. C. Glotzer, Langmuir **21**, 11547 (2005).

[22] N. Kern and D. Frenkel, J. Chem. Phys. **118**, 9882 (2003).

[23] C. Vega, E. Sanz, J. L. F. Abascal, and E. G. Noya, J. Phys.: Condens. Matter **20**, 153101 (2008).

[24] D. Frenkel and A. J.C. Ladd, J. Chem. Phys. **81**, 3188 (1984).

[25] D. A. Kofke, Mol. Phys. **78**, 1331 (1993).

[26] S. J. Singer and R. Mumaugh, J. Chem. Phys. **93**, 1278 (1990).

[27] A. J.C. Ladd and L. Woodcock, Chem. Phys. Lett. **51**, 155 (1977).

[28] A. Z. Panagiotopoulos, Mol. Phys. **61**, 813 (1987).

[29] D. Frenkel and B. Smith, *Understanding Molecular Simulations*, 2nd ed. (Academic, New York, 2001).

[30] P. R. ten Wolde, M. J. Ruiz-Montero, and D. Frenkel, J. Chem. Phys. **104**, 9932 (1996).

[31] A. V. Brukhno, J. Anwar, R. Davidchack, and R. Handel, J. Phys.: Condens. Matter **20**, 494243 (2008).

[32] E. Sanz and D. Marenduzzo, J. Chem. Phys. **132**, 194102 (2010).

[33] C. De Michele, P. Tartaglia, and F. Sciortino, J. Chem. Phys. **125**, 204710 (2006).

[34] W. Dai, C. W. Hsu, F. Sciortino, and F. W. Starr, Langmuir **26**, 3601 (2000).

[35] A. J. Moreno, I. Saika-Voivod, E. Zaccarelli, E. L. Nave, S. V. Buldyrev, P. Tartaglia, and F. Sciortino, J. Chem. Phys. **124**, 204509 (2006).

[36] G. Foffi, E. Zaccarelli, F. Sciortino, and P. Tartaglia, J. Stat. Phys. **100**, 363 (2000).

[37] M. S. Wertheim, J. Stat. Phys. **35**, 19 (1984).

[38] G. Foffi and F. Sciortino, J. Phys. Chem. B **33**, 9702 (2007).

[39] P. R. ten Wolde and D. Frenkel, Science **277**, 1975 (1997).

[40] A. Fortini, E. Sanz, and M. Dijkstra, Phys. Rev. E **78**, 041402 (2008).

[41] P. J. Lu, E. Zaccarelli, F. Ciulla, A. B. Schofield, F. Sciortino, and D. A. Weitz, Nature (London) **453**, 499 (2008).

[42] K. M. Ho, C. T. Chan, and C. M. Soukoulis, Phys. Rev. Lett. **65**, 3152 (1990).

[43] F. García-Santamaría, H. T. Miyazaki, A. Urquía, M. Ibisate, M. Belmonte, N. Shinya, F. Meseguer, and C. López, Adv. Mater. **14**, 1144 (2002).

[44] C. A. Angell, Science **267**, 1924 (1995).

[45] V. Molinero, S. Sastry, and C. A. Angell, Phys. Rev. Lett. **97**, 075701 (2006).

[46] M. H. Bhat, V. Molinero, E. Soignard, V. C. Solomon, S. Sastry, J. L. Yarger, and C. A. Angell, Nature (London) **448**, 787 (2007).